Active Vibration Control of a Beam with Piezoelectric Patches: Real-time Implementation with xPC target

Asan Gani, M.J.E. Salami-*SMIEEE* and Md. Raisuddin Khan

***Abstract*— Active control of a vibrating beam using smart materials such as piezoelectric materials is examined in this paper. A model based on Euler-Bernoulli beam equation has been developed and then extended with bonded three piezoelectric patches which act as sensor, actuator and exciter. The sensor and actuator are collocated to achieve a minimum phase. The aim of this research work is to control the first three resonant modes. To achieve this, a compensated inverse PID controller is developed and tuned to damp these modes using MATLAB. The designed controller for damping each mode is then combined in parallel to damp any of the three modes. Finally, the simulation results are verified experimentally and the real-time implementation is carried out with xPC target toolbox in MATLAB.**

***Index Terms*— Smart Materials, Piezoelectric sensor/actuator, Vibration suppression, Inverse PID, xPC, MATLAB**

I. Introduction

The ability to monitor and control vibration is vital in achieving the desired objectives of many engineering systems, such as automobiles, aerospace, and precision machining and this list could continue. Advances in smart materials have shown an increased interesting application of smart materials for passive and active structural damping. Advancements in smart material technology have produced much smaller actuators and sensors with high integrity in structures. There are significant works in progress to reduce structural vibration. Passive damping treatment has fixed frequency range and adds significant weight to the structures. To overcome these drawbacks *piezoelectric materials* have been advocated for use in order to have control over a wide range of frequencies without adding much weight to the structure. Research in *piezoelectric materials* is rapidly gaining attention in many developed countries and it is envisaged that such technology will widen the scope and enhanced the quality of products in manufacturing industries.

Vibration control using Piezoelectric materials can be accomplished either passively (with shunt circuit) [1]-[3] or actively. In shunt circuit techniques, the main role of piezoelectric material is to dissipate energy. This is achieved when mechanical work is done on an element and some portion of it is converted to and stored as dielectric energy. In a vibrating structure, a shunt network can be configured to accomplish vibration control by modifying the dynamics of the electrical system [4], [5]. This system is analogous to mass-spring dashpot system which acts as a vibration absorber. A properly tuned shunt circuit can add significant damping to a structure. In active control, an external power is applied to a piezoelectric material to produce a force in opposite direction to that produced by vibrating structure at a particular position. The opposite forces will cancel each other and thus reduce its vibration. In this paper, a compensated inverse PID controller is designed to reduce multiple vibration modes of structures. The controller also reduces the 'spillover' effect which is caused by the presence of uncontrolled or unmodeled modes within the bandwidth of the closed loop system.

In this paper piezoelectric materials act as an actuator and a sensor for vibration control of flexible a structure. The results of active control for the first three resonant modes are presented. The controller developed for each mode is tested individually and later combined in parallel to control any of the three modes. The performance of the combined controller is discussed and a comparison is made between the individual and combined controller.

II. Euler-Bernoulli Beam Model: Modal Analysis

In this section, mathematical models for Euler beam as a continuous system and with collocated piezoelectric sensor and actuator are developed. Various transfer functions for use in simulation studies are developed in detail.

A. Lateral Vibration of beam

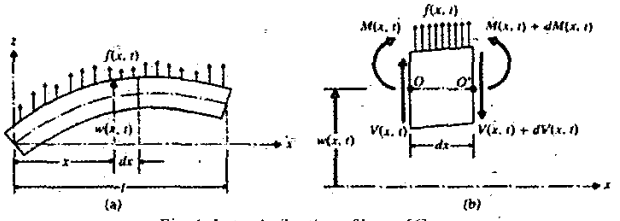

Fig. 1. Lateral vibration of beam [6]

Manuscript received January 17, 2003. This work has been supported in part by the IIUM Research Centre under Intensification of Research in Priority Area (IRPA) Grant.

The authors are with Departments of Mechatronics Engineering, Faculty of Engineering, International Islamic University Malaysia, Jalan Gombak, 53100, Kuala Lumpur. (tel: +603 – 2056 4419, fax: +603-2056 4853; e-mail: asan@iiu.edu.my; momoh@iiu.edu.my; raisuddin@iiu.edu.my).

Inertia force acting on beam = $\rho A(x)dx\frac{\partial^2 z(x,t)}{\partial t^2}$ where ρ = mass density, $A(x)$ = cross sectional area and $\rho A(x)$ = mass per unit length. Considering the equation of motion along the z-axis and the moment around y-axis at O leads to:

$$-(V+dV)+f(x,t)dx+V=\rho A(x)dx\frac{\partial^2 z(x,t)}{\partial t^2} \quad (1)$$

$$(M+dM)-M-(V+dV)dx+f(x,t)dx\frac{dx}{2}=0 \quad (2)$$

Taking $dV=\frac{\partial V}{\partial x}dx$, $dM=\frac{\partial M}{\partial x}dx$ and $(dx)^2=0$, then equation becomes:

$$-\frac{\partial^2 M}{\partial x^2}(x,t)+f(x,t)=\rho A(x)\frac{\partial^2 z(x,t)}{\partial t^2} \quad (3)$$

Based on Euler-Bernoulli or thin beam theory the relationship between bending moment and deflection is given by:

$$M(x,t)=EI(x)\frac{\partial^2 z}{\partial x^2}(x,t) \quad (4)$$

where E=Young's modulus and I(x) is the area moment of inertia of the beam cross section about the neutral axis. Substituting (4) in (3) gives:

$$EI(x)\frac{\partial^4 z}{\partial x^4}(x,t)+\rho A(x)\frac{\partial^2 z(x,t)}{\partial t^2}=f(x,t) \quad (5)$$

B. Model of beam with bonded piezoelectric patches

Fig. 2 shows the position of the attached piezoelectric patch on beam. The piezoelectric actuator's dimension is as shown in the figure and a voltage $V_a(t)$ is applied to it.

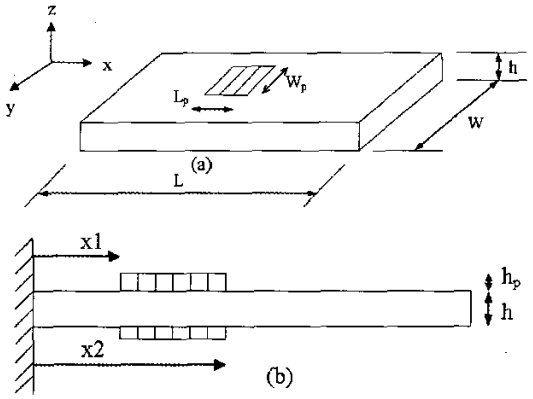

Fig. 2. Collocated piezoelectric patches on the beam

Assuming the beam is a one dimensional system, equation (5) becomes:

$$EI(x)\frac{\partial^4 z}{\partial x^4}(x,t)+\rho A(x)\frac{\partial^2 z(x,t)}{\partial t^2}=\frac{\partial^2 M_a}{\partial x^2}(x,t) \quad (6)$$

where M_a is the actuator induced bending moment. If the beam is bent by an external load into downward curvature the portion of the beam and piezo actuator above the neutral axis will experience tension. The moment M_a is given by:

$$M_a=\overline{K}V_a(t) \quad (7)$$

$$\overline{K}=\frac{E_b I\kappa d_{31}}{h_a} \text{ and } \kappa=\frac{12E_a h_a\left[h+h_a\right]}{\left[2E_b h^3+E_a\left[(h+2h_a)^3-h^3\right]\right]}$$

To incorporate the placement of the piezo patch on the beam surface in x direction, Heaviside Step function is employed, so that the finite length of actuator, (7) can be written as:

$$M=\overline{K}V_a(t)\left[H(x-x_1)-H(x-x_2)\right] \quad (8)$$

Substituting $z(x,t)=\sum_{k=1}^{\infty}w_k(x)q_k(t)$ and (8) in (6) yields:

$$\frac{\partial^2 q_k(t)}{\partial t^2}+\omega_k^2 q_k(t)=\frac{\overline{K}V_a(t)}{\rho A(x)}\left(w_k'(x_2)-w_k'(x_1)\right) \quad (9)$$

C. Transfer functions for simulation studies

Taking the Laplace transform of equation (9) gives:

$$q_k(s)\left[s^2+\omega_k^2\right]=\frac{\overline{K}\left(w_k'(x_2)-w_k'(x_1)\right)}{\rho A(x)}V_a(s) \quad (10)$$

Since, $z_k(x,s)=w_k(x)q_k(s)$ equation (10) becomes:

$$z_k(x,s)=\frac{w_k(x)\overline{K}\left(w_k'(x_2)-w_k'(x_1)\right)}{\rho A(x)\left[s^2+\omega_k^2\right]}V_a(s) \quad (11)$$

The transfer function that describes the elastic deflection of the entire beam due to an applied voltage to the actuator is given in (11). Incorporating a proportional damping term [7] to (11) gives:

$$G_{vaz}(x,s)=\frac{z_k(x,s)}{V_a(s)}=\sum_{k=1}^{\infty}\frac{\left(\overline{K}/\rho A(x)\right)w_k(x)\left(w_k'(x_2)-w_k'(x_1)\right)}{\left[s^2+2\zeta_k\omega_k s+\omega_k^2\right]} \quad (12)$$

2) Piezoelectric sensor voltage vs. piezoelectric actuator voltage: Using Hooke's law for beam deflection in x directions, the strain experienced by the sensor patch is obtained as [8] :

$$\varepsilon_b(x,t)=\frac{\partial u}{\partial x}=-\left(\frac{h}{2}+h_p\right)\frac{\partial^2 z(x,t)}{\partial x^2} \quad (13)$$

The strain introduced in the beam will produce an electric charge distribution per unit area in piezo sensor due to piezoelectric effect. The electric charge distribution is given by $q(x,t)=\frac{k_{31}^2}{g_{31}}\varepsilon_b$ where k_{31} is the electromechanical coupling constant and g_{31} is the piezoelectric stress constant. The total charge accumulated on the sensing layer can be found by integrating q(x,t) over the entire surface area of the piezo sensor and that is given by,

$$Q(t)=\int_{x1}^{x2}w_p q(x,t)dx=-w_p\left(\frac{h}{2}+h_a\right)\frac{k_{31}^2}{g_{31}}\frac{\partial z(x,t)}{\partial x}\Big|_{x1}^{x2} \quad (14)$$

Charged piezoelectric patches can be considered as a parallel plate capacitor, the voltage across the layer will be;

$$V_s(t)=\frac{Q(t)}{C_p(x2-x1)}=C_s\frac{\partial z(x,t)}{\partial x}\Big|_{x1}^{x2} \quad (15)$$

Where C_p is the patch capacitance and x2-x1 is the length of piezo sensor and C_s is:

$$C_s=-w_a\left(\frac{h}{2}+h_a\right)\frac{k_{31}^2}{C_p g_{31}(x2-x1)}$$

Taking the Laplace transform of (15) gives

$$V_s(s) = \frac{C_s \overline{K}}{\rho A(x)} \sum_{k=1}^{\infty} \frac{\left(w_k'(x2) - w_k'(x1)\right)\left(w_k'(x2) - w_k'(x1)\right)}{\left[s^2 + 2\zeta_k \omega_k s + \omega_k^2\right]} V_a(s)$$

which can be written as

$$G_{vavs}(s) = \frac{V_s(s)}{V_a(s)} = \frac{C_s \overline{K}}{\rho A(x)} \sum_{k=1}^{\infty} \frac{\left(w_k'(x2) - w_k'(x1)\right)^2}{\left[s^2 + 2\zeta_k \omega_k s + \omega_k^2\right]} \quad (16)$$

3) Piezoelectric exciter voltage vs. piezoelectric sensor voltage and beam deflection: Fig. 3, shows the piezoelectric exciter's location on the beam, where the applied force F(x,t), which depends on the applied voltage, $V_e(t)$ is used to excite the piezoelectric patch.

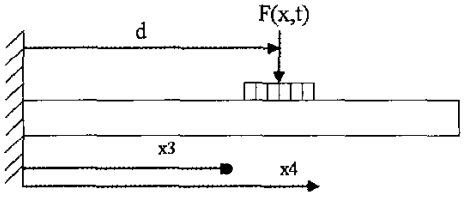

Fig. 3. Location of piezoelectric exciter on beam

From (10), the sensor voltage output for applied exciter voltage is given by

$$V_s(s) = C_s \sum_{k=1}^{\infty} \frac{\overline{K}\left[w_k'(x4) - w_k'(x3)\right]\left[w_k'(x2) - w_k'(x1)\right]}{\rho A(x)\left[s^2 + 2\zeta_k \omega_k + \omega_k^2\right]} V_e(s) \quad (17)$$

resulting in

$$G_{vevs}(s) = \frac{V_s(s)}{V_e(s)} = C_s \sum_{k=1}^{\infty} \frac{\overline{K}\left[w_k'(x4) - w_k'(x3)\right]\left[w_k'(x2) - w_k'(x1)\right]}{\rho A(x)\left[s^2 + 2\zeta_k \omega_k + \omega_k^2\right]} \quad (18)$$

$$G_{vez}(s) = \frac{z(x,s)}{V_e(s)} = \sum_{k=1}^{\infty} \frac{\overline{K} w(x)\left[w_k'(x4) - w_k'(x3)\right]}{\rho A(x)\left[s^2 + 2\zeta_k \omega_k + \omega_k^2\right]} \quad (19)$$

III. CONTROLLER DESIGN AND SIMULATION RESULTS

A. Block diagram for beam with attached piezoelectric patches

The structure of the closed loop system of the beam attached with piezoelectric sensor and actuators is shown in Fig. 5 and Fig. 6. In Fig. 6, an extra transfer function $G_{zvs}(s)$ is introduced to transfer tip displacement to piezoelectric sensor voltage output. This is necessary since the reference input is in voltage.

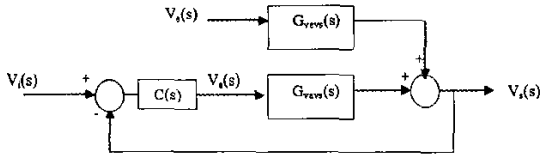

Fig. 5. Block diagram with feedback control for piezoelectric Sensor ($V_s(s)$)

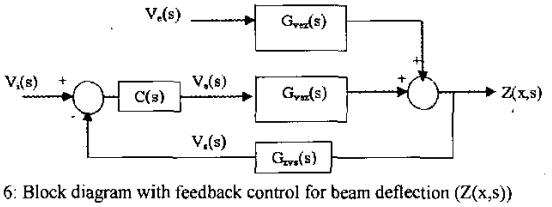

Fig. 6: Block diagram with feedback control for beam deflection (Z(x,s))

The actuator voltage $V_a(s)$ is $V_a(s) = [V_i(s) - V_s(s)]C(s)$. The block diagram reduction for Fig. 5 and Fig. 6 lead to the close loop transfer functions as follows;

$$V_s(s) = \frac{G_{vevs}(s)V_e(s)}{1 + C(s)G_{vavs}(s)} + \frac{C(s)G_{vavs}(s)V_i(s)}{1 + C(s)G_{vavs}(s)} \quad (20)$$

$$Z(x,s) = \frac{G_{vez}(s)V_e(s)}{1 + C(s)G_{vaz}(s)G_{zvs}(s)} + \frac{C(s)G_{vaz}(s)Z_i(x,s)}{1 + C(s)G_{vaz}(s)G_{zvs}(s)} \quad (21)$$

since $G_{vavs}(s) = G_{vaz}(s)G_{zvs}$, (21) is reduced to

$$Z(x,s) = \frac{G_{vez}(s)V_e(s)}{1 + C(s)G_{vavs}(s)} + \frac{C(s)G_{vaz}(s)Z_i(x,s)}{1 + C(s)G_{vavs}(s)} \quad (22)$$

It is desired to have $V_i(s)$ equal to zero and the role of the controller is only to eliminate the effects of the disturbance force F(x,t). Since a piezoelectric actuator is used as an exciter, the input force is controlled by its voltage $V_e(s)$.With $V_i(s) = 0$, diagram in Fig. 5 reduced to Fig.7 and transfer functions (20) and (21) can also be simplified.

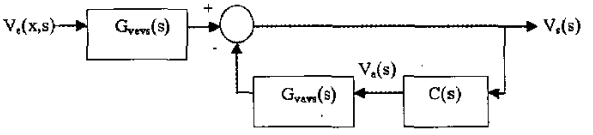

Fig. 7. Block diagram with feedback control for sensor output when $V_i(s)=0$

B. Controller design

The proposed controller in this paper is 'compensated inverse PID' or denoted as CIPID that takes the following form. The subscript 'i' stands for number of modes. The controller is developed by taking into consideration the effect of truncated modes which might cause the spillover effects [9],[10]. Hence the controller is designed to attenuate first three modes so that

$$C_i(s) = \sum_{i=1}^{3} \frac{s\left(\frac{1}{K_D}\right)_i \left(s + \frac{K_P}{K_D}\right)_i}{s^2 + \left(\frac{K_P}{K_D}\right)_i s + \left(\frac{K_I}{K_D}\right)_i} \quad (25)$$

where K_P, K_I and K_D are respectively the gains of the PID and these are tuned to damp i-th mode, where ω_i is the resonant frequency for i-th mode, that is

$$\left(\frac{K_I}{K_D}\right)_i = \omega_i^2, \left(\frac{K_P}{K_D}\right)_i = 2\zeta\omega_i \quad (26)$$

Using superposition rules, the CIPID controller can be extended to control first three modes as given in (25). The controller for each mode will be arranged in parallel. Basically the CIPID is used to damp the resonant peaks by placing poles at each resonant frequency. Changing K_P in the above equation will change the damping factor for each mode and can control the resonant peak. However higher damping factor doesn't mean that the peak will be always reduced; hence an optimal value of K_P is required for each mode. Fig. 8, shows the controller and beam with bonded piezoelectric. A digital

lowpass filter is applied to sensor output to remove any interference signal or noise.

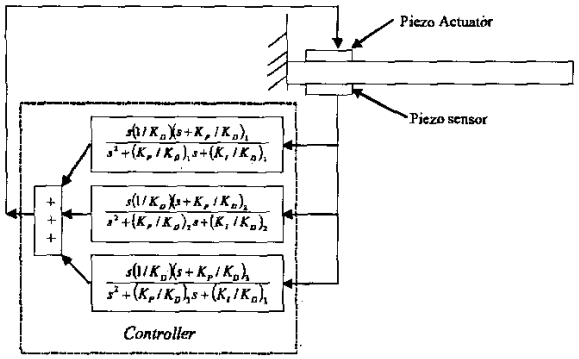

Fig. 8. Controller and beam bonded with piezoelectric patches

C. *Simulation results*

The ability of the above controller in damping the resonant modes is investigated here. Different values of K_P, K_I and K_D are taken to study their effects on the resonant modes. Initial simulation is carried out for the individual modes and the individual controllers are combined to damp all the three modes. In order to get more realistic simulation results, the damping factors and modes frequencies used for simulations in equations (12), (16), (18) and (19) are taken from the experimental results. The experimental damping ratios and mode frequencies are shown in Table I.

TABLE I
EXPERIMENTAL MODE FREQUENCIES AND ITS DAMPING RATIOS

Modes	Frequency	ζ (damping ratio)
1	11.14	0.02027
2	66.74	0.01021
3	186.64	0.00520

In this simulation studies, the value of K_D is chosen to be 1, K_I is taken from equation (26) and K_P is adjusted by taking different values of zeta in equation (26). The simulation is carried out by changing the value of K_P which correspondingly varies the damping ratio of the controller. The optimal values of K_P can then be obtained. The results obtained for resonant peak reductions for V_s are summarized in Table II.

TABLE II
SIMULATION RESULTS FOR PEAK REDUCTIONS (DB) FORFIRST THREE MODES

Zeta	Kp	First Mode	Second Mode	Third Mode
10	222.82	3.33	0.4	0.1
5	111.41	5.6	1.9	0.7
1	22.282	14.61	3.4	1.3
0.5	11.141	**18.676**	5	**2.9**
0.1	2.2282	15.121	**11.46**	11.5
0.01	0.2228	14.05	18.38	-22.1

This table shows maximum reduction for the first mode at zeta = 0.5 or K_P = 11.141. Smaller values of zeta cause undesirable shift of the resonant frequency and introduce new peaks at the neighborhood of the actual frequency. For the second mode, greater reduction is achieved for zeta=0.01. However, this value introduces new peak on the left side of the resonant frequency, hence the most suitable value of K_P is 2.2282. For the third mode, lower damping values increase the resonant peak, instead of reducing it, hence the best result is achieved with K_P = 11.141.

IV. EXPERIMENTAL SETUP AND DATA ACQUISITION SYSTEM

This section discusses the instruments, data acquisition systems and software used for implementation of active vibration control in real-time. Properties of hardware are also discussed in detail. An aluminum beam is used to carry out the experiment. The properties of the beam are given in Table III.

TABLE III
PROPERTIES OF BEAM (6061 T651)

Parameter	Value	Unit
Length, L	0.5	m
Width, w	0.04	m
Thickness, h	0.003	m
Modulus of Young, E	6.9×10^{10}	N/m^2
Area Moment of Inertia, I	9×10^{-11}	m^4
Density, ρ	2700	kg/m^3
Area, A	1.2×10^{-4}	m^2

Three ACX piezoelectric patches are used in this research. Two unimorph patches model QP10W are collocated and used as sensor and actuator. One bimorph patch model QP25N is used as an exciter. Their properties are given in Table IV.

TABLE III
PROPERTIES OF PIEZOELECTRIC PATCHES

Parameter	Units	QP 10 W (sensor/actuator)	QP 25 N (Exciter)
Length, L_p	mm	45.974	45.974
Width, w_p	mm	33.274	20.574
Height, h_p	mm	0.254	0.127
Capacitance	μF	0.1	0.2
Coupling Coefficient, k_{31}		0.3	0.4
Elastic Modulus, E_{11}	Pa	6.9×10^{10}	6.3×10^{10}
Elastic Modulus, E_{31}	Pa	5.5×10^{10}	5×10^{10}
Charge Coefficient, d_{31}	m / V	-179×10^{-12}	-285×10^{-12}

The piezoelectric exciter is placed at the middle of the beam. While the piezoelectric actuator and sensor are collocated near the fix end of the beam. The transfer function of a collocated sensor-actuator has minimum phase due to pole-zero interlacing [11], [12]. To add the most damping, the piezoelectric patch is bonded on the structure in the area of highest strain energy. It is as been reported in [3], [14] that the highest strain energy for first three modes is at clamped boundary of the cantilever beam. Reference [14] showed that analytical equation can be used accurately to predict the optimum position of piezoelectric. The piezoelectric sensor and actuator are attached at about 15 mm from the clamped end of the beam.

Two linear power amplifiers are used in this setup. Both amplifiers have a gain up to 20 and output voltage of ±200V.

A Keyence laser displacement sensor model LK-081 is used to measure the beam tip displacement. National instruments (NI) data acquisition card model PCI-MIO-16XE-10 is used to acquire analog signal from the piezoelectric sensor. Control signal is sent to piezoelectric actuator through output channel of the card. A four channel HP-Dynamic signal analyzer (DSA) model HP-35670A, is used to obtain beam resonant frequencies and respective damping ratios. Controlled and uncontrolled responses of the beam are measured and analyzed using the DSA.

Real-time implementation is carried out using xPC Target toolbox in MATLAB. It is a high-performance, host-target prototyping environment that enables the connection or Simulink models to physical systems and execute them in real-time on PC-compatible hardware [15]. xPC target enables to add I/O blocks to Simulink models, automatically generate code with Real-time Workshop, and download the code to a second PC running the xPC Target real-time kernel.

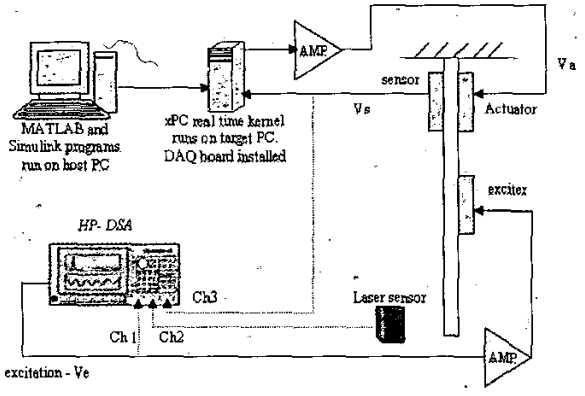

Fig. 9. The experimental setup for active vibration control.

HP-DSA is used to obtain transfer functions under controlled and uncontrolled condition. Ch2/Ch1 gives transfer function for beam tip displacement to input excitation signal (G_{vez}) and Ch3/Ch1 will measure transfer function for piezo-sensor output to input excitation signal (G_{vevs}).

V. Experimental Results

In this section we will experimentally verify the controllers' performances. Early results have shown the individual controller performance in damping respective modes. Thereafter the controller is combined to damp all the three modes. The experimental results of this combined controller are discussed toward the end of this section

A. First mode controller's performance

The beam is excited at its first resonant frequency which is 11.141 Hz in order to test the controller ability in damping this mode. Fig. 10(a) and Fig. 10(b) are showing the gain of G_{vevs} and piezoelectric sensor output (V_s) respectively under controlled and uncontrolled conditions.

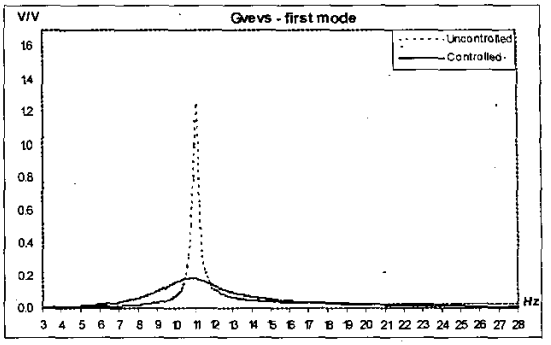

Fig. 10(a) : Controlled and uncontrolled gain for G_{vevs} at first mode

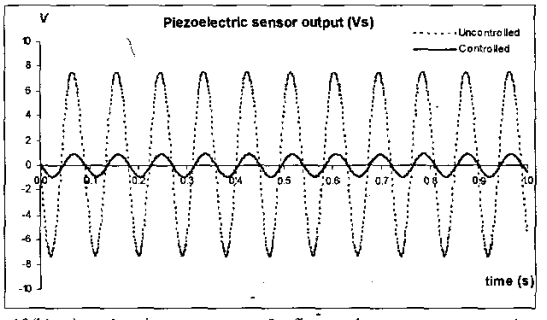

Fig. 10(b): piezoelectric sensor output for first mode

Fig. 11(a) shows the reduction in gain of G_{vez} while Fig. 11(b) shows in reduction in peak-peak beam tip displacement upon switching on the controller.

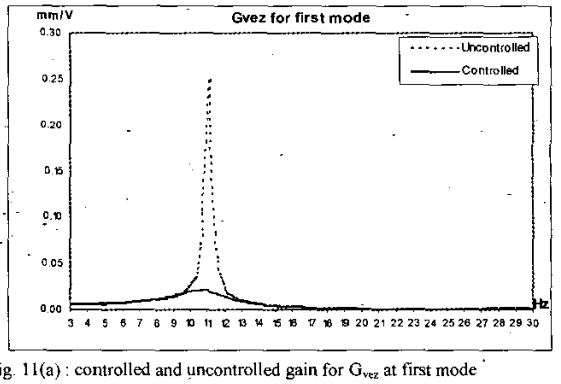

Fig. 11(a) : controlled and uncontrolled gain for G_{vez} at first mode

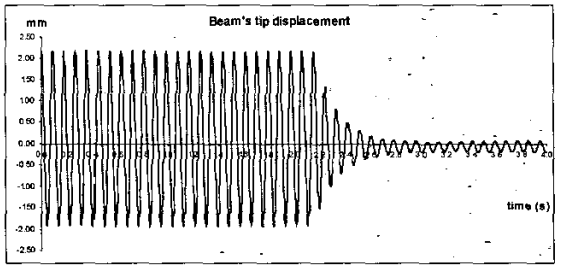

Fig. 11(b): Peak-peak displacement of beam tip at first mode

The first mode controller's performance is summarized in Table V:

TABLE V
PERFORMANCE OF THE FIRST MODE CONTROLLER

	Gvevs *(V/V)*	Vs *(volt)*	Gvez *(mm/V)*	z *(mm)*
Uncontrolled	1.2496	7.472	0.24980	2.562
Controlled	0.1765	0.878	0.01987	0.678
Reduction	1.0731	6.594	0.22993	1.884
Reduction (dB)	**17.00**	**18.60**	**22.00**	**11.55**
Reduction (%)	**92.05**	**73.54**	**85.88**	**88.25**

B. Second mode controller's performance

The beam is excited at 66.744 Hz to produce second resonant mode. The controller's ability to damp second mode is demonstrated in Fig. 12 and 13. Fig. 12 shows the reduction in gain for G_{vevs}.

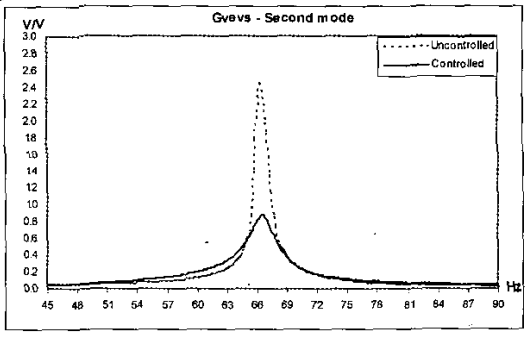

Fig. 12: Controlled and uncontrolled gain for G_{vevs} at second mode,

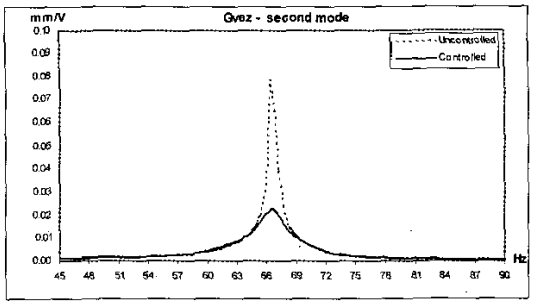

Fig. 13: controlled and uncontrolled gain for Gvez at second mode

TABLE VI
PERFORMANCE OF THE SECOND MODE CONTROLLER

	Gvevs*(V/V)*	Vs*(volt)*	Gvez *(mm/V)*	z *(mm)*
Uncontrolled	2.4594	9.9517	0.07837	0.275
Controlled	0.8817	4.1592	0.02266	0.08177
Reduction	1.5777	5.7925	0.05571	0.19323
Reduction (dB)	**8.910**	**7.58**	**10.78**	**10.53**
Reduction (%)	**64.15**	**58.21**	**71.09**	**70.27**

C. Third mode controller's performance

The performance of third mode controller is shown in Fig. 14. The beam is excited at 186.6 Hz.

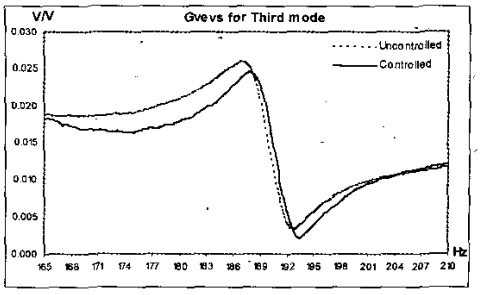

Fig. 14: Controlled and uncontrolled gain for Gvev at third mode

The peak reduction for third mode is shown in Table VII :

TABLE VII
PERFORMANCE OF THE THIRD MODE CONTROLLER

	Gvevs *(V/V)*	Vs *(volt)*
Uncontrolled	0.02583	0.0921
Controlled	0.02374	0.0695
Reduction	0.00209	0.0226
Reduction (dB)	**0.73287**	**2.4455**
Reduction (%)	**8.10**	**24.54**

D. Combined controller's performance

Individual mode controllers are combined in parallel to form a new combined controller. The performance of this combined controller is discussed in this section. The beam is excited with sweep sine signal over frequency range of 3 to 203 Hz, which comprises first three resonant mode frequencies. The controlled and uncontrolled transfer function G_{vez} and G_{vevs} are shown in Fig. 15 and Fig. 16 consecutively

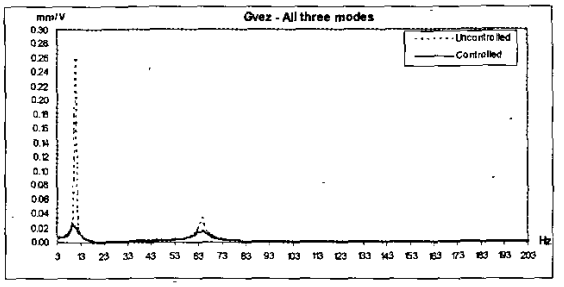

Fig. 15: Controlled and uncontrolled gain for G_{vez} for first three modes

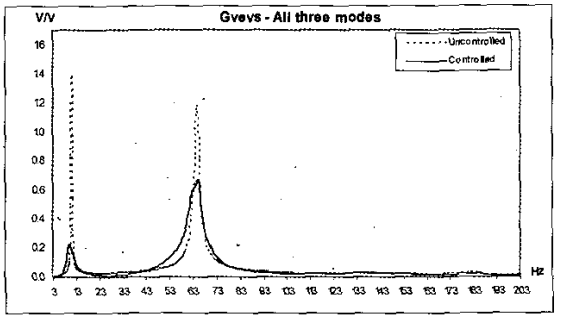

Fig. 16: Controlled and uncontrolled gain for G_{vevs} for first three modes

The summary of peak reduction for combined controller is given in Table VIII. The third mode for G_{vez} is not visible due to negligibly small gain.

TABLE VIII
PERFORMANCE OF THE COMBINED CONTROLLER

	Gvez *(mm/V)*			Gvevs *(V/V)*		
mode	1st	2nd	3rd	1st	2nd	3rd
Uncontrolled	0.2584	0.0348	-	1.3879	1.1888	0.0294
Controlled	0.0191	0.0148	-	0.1945	0.5417	0.0280
Reduction	0.2394	0.02	-	1.1934	0.6471	0.0014
Reduction (dB)	**22.65**	**7.41**	-	**17.07**	**6.8270**	**0.4240**
Reduction (%)	**92.63**	**57.41**	-	**86.00**	**54.43**	**4.76**

Table IX, shows the reduction in dB for first, second and third modes under the effects of individual and combined controller

TABLE IX
REDUCTION FOR INDIVIDUAL AND COMBINED CONTROLLER

	Individual controller		**Combined controller**	
mode	Gvez	Gvevs	Gvez	Gvevs
1st	*22.00*	*17.00*	*22.65*	*17.07*
2nd	*10.78*	*8.91*	*7.41*	*6.827*
3rd	-	*0.73*	-	*0.424*

VI. CONCLUSION

This paper has discussed the use of piezoelectric materials to control the vibration of a beam. A novel controller that is based on inverse PID has been designed and used to achieve this objective. The results of the real-time implementation of the controller using xPC target are found to be very close to that of simulation studies which actually demonstrates the effectiveness of this technique. In general, the combined controller has shown a better performance for G_{vez} for the first mode while it slightly produces poorer performance for the second mode as compared to the performance of the individual controller. However for G_{vevs}, the individual controller has shown greater performance over the combined controller for all the three modes. The drop in the performance for combined controller is likely due to the coupling effects and further research work on this aspect is under investigation.

REFERENCES

[1] Hagood, N.W., and von Flotow, A.H., "Damping of Structural Vibrations with piezoelectric Materials and Passive Electrical Network" Journal of Sound and Vibration, 146(2), 1991

[2] S Y Wu, " Method for multiple mode shunt damping of structural vibration using single PZT transducer", Proceedings SPIE, Smart Structures and Intelligent System, March 1998

[3] John J. Granier, Jason Hundhausen, and Gabriel E. Gaytan, "Passive Modal Damping with Piezoelectric Shunts", Los Alamos National Labs, 2001

[4] Giovanni Caruso, "A critical analysis of electric shunt circuits employed in piezoelectric passive vibration damping", Smart materials and structures, 2001

[5] H. R Pota, S O Reza Moheimani and Matthew Smith, "Resonant controller for smart structures", Smart Materials and Structures, 2002

[6] Singiresu S. Rao, "Mechanical Vibrations", Addison Wesley, 1995.

[7] S. O. Reza Moheimani, "Experimental Verification of the Corrected Transfer Function of A Piezoelectric Laminate Beam", IEEE Transactions on Control Systems Technology, Vol. 8, 2000.

[8] C. R. Fuller, S. J. Elliott & P.A. Nelson, "Active Control of Vibration", Academic Press, 1996.

[9] R. L. Clark, "Accounting for out-of-bandwidth modes in the assumed modes approach: Implications on collocated output feedback control," Trans. ASME J. Dynamic System., Measurement, Contr., vol. 119, 1997

[10] Reza Moheimani, S.O and Clark, R.L., "Minimizing the truncation error in assumed modes models of structures", American Control Conference, V4, 2000

[11] Robert L. Clark, William R. Saunders and Gary PP. Gibbs, "Adaptive Structures", John Wiley & Sons, 1998.

[12] Mark McEver and Donald J. Leo, "Autonomous Vibration Suppression Using On-Line Pole-Zero identification", Journal of Sound and Acoustics, 2001

[13] Law H.H., Rossiter, P.L., Simon, G.P., and Koss, L.L., "Characterization of Mechanical vibration damping by piezoelectric materials", Journal of Sound and Vibration, Vol. 197, 1996

[14] *xPC Target Selecting Hardware Guide-Manual*, MathWorks, 2001

Asan Gani is from Malaysia, was born in 71. He received his B.Eng. in Mechatronics Engineering (First Class Honors) from International Islamic University Malaysia (IIUM), in 2000. Asan Gani he is an assistant lecturer at IIUM, and at the final stage of completing his M.Sc. in Mechatronics Engineering. His current research is in active vibration control using piezoelectric materials. He is an associate member of IEEE

Momoh Jimoh E Salami received his B.S.E.E degree from University of Ife, Nigeria in June 1977, postgraduate diploma from Philips International Institute for Technological Studies, Eindhoven, Netherland in Dec. 1979 and PhD. from University of Calgary, Canada in June 1985. He has a wide teaching experience in many high academic institutions in various countries. He joined IIUM in Sept. 1996 and is currently the Head of Department of Mechatronics Engineering. He has authored or co-authored more than 50 publications including textbook, journals and conference papers. His research interests include intelligent system design and digital signal and image processing. Prof. Dr. Momoh is a senior member of IEEE

Md Raisuddin Khan, Md. Raisuddin Khan was born in Bangladesh in January 1960. He received his PhD in Mechanical engineering in 1996 from the Bangladesh University of Engineering and Technology (BUET). He is currently Associate Professor in the Mechatronics Engineering Department of the International Islamic University Malaysia (IIUM). Before joining IIUM in January 2001 he was Associate Professor and Head of the Mechanical Engineering Department in the Bangladesh Institute of Technology (BIT), Chittagong. He comes with a background in applied mechanics, especially in the area of stress and stability analyses of elastic structures. Presently he is conducting research on active shape and vibration control of composite structures